

DINE: Dimensional Interpretability of Node Embeddings

Simone Piaggese, Megha Khosla, André Panisson, and Avishek Anand



Abstract—Graphs are ubiquitous due to their flexibility in representing social and technological systems as networks of interacting elements. Graph representation learning methods, such as node embeddings, are powerful approaches to map nodes into a latent vector space, allowing their use for various graph tasks. Despite their success, only few studies have focused on explaining node embeddings locally. Moreover, global explanations of node embeddings remain unexplored, limiting interpretability and debugging potentials. We address this gap by developing human-understandable explanations for dimensions in node embeddings. Towards that, we first develop new metrics that measure the global interpretability of embedding vectors based on the marginal contribution of the embedding dimensions to predicting graph structure. We say that an embedding dimension is more interpretable if it can faithfully map to an understandable sub-structure in the input graph - like community structure. Having observed that standard node embeddings have low interpretability, we then introduce DINE (Dimension-based Interpretable Node Embedding), a novel approach that can retrofit existing node embeddings by making them more interpretable without sacrificing their task performance. We conduct extensive experiments on synthetic and real-world graphs and show that we can simultaneously learn highly interpretable node embeddings with effective performance in link prediction.

1 INTRODUCTION

Node embeddings are general purpose low-dimensional, continuous vertex representations in dense vector spaces. These embeddings are typically learned by trying to optimize a user-defined or flexible notion of structural similarity between vertices. Node embeddings have proven to be mature and popular techniques with widespread applications in web and social network analysis tasks like link prediction and community detection to name a few [1] due to their simplicity, and expressive power. However, one of their shortcomings is the innate lack of interpretability of the latent vector spaces they exist in. Specifically, each of the learned latent dimensions does not have a corresponding realizable interpretation in the input graphs [2]–[4]. This paper aims to fill this critical gap by proposing a method to retrofit “already learned” non-interpretable embeddings into a new and interpretable vector space without compromising the task performance.

The meaning of individual latent embedding dimensions is hard to define and determine [2]–[4]. We operate on a general, yet powerful notion of grounding the interpretation of each dimension to understandable sub-structures of the input graphs, e.g., communities, subgraphs, etc. This design decision has clear advantages in downstream tasks where sub-graphs or communities are clear explanations of a predictive task. As a concrete example, in a link-prediction task the likelihood of a link is higher for a pair of nodes in the same community [5]. Similarly, in several bio-medical tasks that use embedding features like [6], [7], subgraphs refer to a protein or genetic pathways. Therefore, automatically grounding latent dimensions to sub-graphs and community structures will improve understanding of the prediction process.

Existing literature investigating the interpretability of node embeddings is limited to three major aspects. First, posthoc feature-attribution methods like [8]–[10] explain a decision in terms of (a) subset of node features or (b) nodes/edges in the computational graph. If embeddings are used as features, subsets of latent features are still non-interpretable. Explaining a prediction in terms of edges and nodes is a useful first step, but these approaches cannot be used globally. Specifically, the meaning of a latent dimension can still not be explained using these local methods. Secondly, in the presence of ground-truth node labels [4], [11] measure the interpretability of embedding dimensions in terms of their association strength with these labels without providing an explicit explanation like our approach. These approaches pre-suppose a certain interpretable mapping and are not flexible. Finally, [12] search for interpretable subspaces related to concepts from knowledge bases. Unlike earlier works, we operate on a more generalized setting extracting explanations that are agnostic to ground truth labels. Additionally, and more importantly, we propose methods that retrofit existing node embeddings to make their dimensions more interpretable.

In this work, the central aim is finding the human-interpretable meaning of node embedding dimensions and associating latent directions with understandable structural features of the input graph. Despite this *post-hoc* approach, we cannot rely on existing tools for interpreting prediction models [13], [14], mainly because they are designed for supervised tasks. Instead, we analyze unsupervised node embeddings to find evidence for interpretable latent units associated with individual semantic concepts of the input

- S. Piaggese is with University of Pisa, Italy.
Email: simone.piaggese@di.unipi.it
- A. Panisson is with CENTAI Institute, Italy.
- M. Khosla and A. Anand are with TU Delft, Netherlands.

data. Since many empirical graphs are characterized by an underlying community structure [15], we associate communities as interpretable semantic concepts of the input data. We first develop a metric for interpreting each dimension of the node embeddings in terms of its utility in predicting edges in the graph.

Our utility measure $-\mu_d(\mathbf{u}, \mathbf{v})$ is based on feature removal methods and expresses the individual contribution of dimension d for predicting edge (u, v) from embeddings. Using this measure, we can construct saliency maps (refer to Figure 1), to recognize groups of edges (salient subgraphs) that are reconstructed by specific dimensions. We then define quantitative metrics to estimate the interpretability of latent dimensions: we assess interpretability as a “degree of association” with individual graph communities and the sparsity level for these associations. As an example, in Figure 1(a), we sort DEEPWALK dimensions according to our metrics of interpretability, showing that the majority of units are not immediately interpretable since they do not match with a single clique of the synthetic graph.

Secondly, we propose a novel and modular approach, called DINE, to post-process existing node representations and enhance their interpretability. DINE embeds input embeddings into a new sparse, interpretable, and low-entropy vector space. Figure 1(b) shows the result of this post-processing step on DEEPWALK vectors. DINE also preserves the topological graph information to be employed in usual downstream tasks with minimal performance loss.

In our extensive experimental evaluations, we compare our approach with other embedding methods in terms of interpretability, link prediction performance, and scalability over multiple real-world graph datasets. Our results show that DINE convincingly, under most experimental conditions, outperforms existing baselines in terms of dimensional interpretability with negligible to no performance losses. To summarize, our main contributions are as follows:

- We formalize the desirable properties for global explanations of node embeddings, namely *decomposability*, *comprehensibility*, and *sparsity*.
- We introduce a new utility measure that allows the extraction of explanatory subgraphs, one for each dimension (addressing the property of Decomposability). Our measure is grounded in feature attribution techniques like the Shapley value, which are widely used for removal-based explanations. Moreover, we propose two metrics to measure Comprehensibility and Sparsity of explanatory subgraphs.
- We propose a novel, modular, and theoretically sound method DINE that intends to retrofit existing node embeddings to improve their global interpretability.
- We run extensive experimental analyses to establish clear gains in the interpretability-performance trade-offs using DINE.

Our code and artifacts will be released at <https://www.github.com/simonepiaggese/dine>.

2 PRELIMINARIES AND RELATED WORK

2.1 Preliminaries and Notation

Given an undirected, unattributed and unweighted graph $\mathcal{G} = (\mathcal{V}, \mathcal{E})$, node embeddings are the output of an encoder

function

$$e : v \in \mathcal{V} \mapsto \mathbf{e}(v) = \mathbf{v} \in \mathbb{R}^D \quad (1)$$

which map nodes into geometric points of the D -dimensional vector space \mathbb{R}^D (usually $D \ll |\mathcal{V}|$). We will refer to both $\mathbf{e}(v)$ and \mathbf{v} as the embedding vectors of node $v \in \mathcal{V}$ mapped through the encoder e , and with $e_d(v)$ and v_d as entries of these vectors corresponding to dimension d . Usually embedding vectors are collected into the columns of the embedding matrix $\mathbf{X} \in \mathbb{R}^{D \times |\mathcal{V}|}$, i.e. $X_{d,v} = e_d(v) = v_d$. Later we will refer to D as the cardinality of the set $\mathcal{D} = \{1, \dots, D\}$ containing the enumerated dimensions.

In the case of DEEPWALK [17] and NODE2VEC [18], the encoder is a lookup function where node representations are learned through the optimization of a neighborhood reconstruction loss. Specifically, the output of a decoder $\text{DEC} : \mathbb{R}^D \times \mathbb{R}^D \rightarrow \mathbb{R}$ is optimized to predict node pairs $(u, v) \in \mathcal{T} \subseteq \mathcal{V} \times \mathcal{V}$ generated from co-occurrences in unbiased or biased random walks. Many other embedding methods fit this *encoder-decoder* framework [19]: for example, factorization-based embeddings [20], [21] and even deep neural networks methods like [22], where the encoder function is given by a graph convolutional network [23].

2.2 Related Work

Interpretability for node embeddings. From the node embeddings perspective, interpretability is a multi-faceted concept that has been studied from different angles. In [3], [24] authors investigate, using prediction tasks, whether specific topological graph features (e.g. degree centrality, clustering coefficient, etc.) are encoded into node representations. These works significantly differ from our approach, where the aim is to find the comprehensible meaning of embedding dimensions, associating single dimensions with interpretable graph structures (e.g. communities). Other methods focus on measuring interpretability of node embeddings with respect to node labels [4] and node centralities [25]. In [2] global interpretations are given as a hierarchy of graph partitions, but they do not focus on interpreting single dimensions. In [26] the authors study the impact on learned node embeddings when removing edges from the input graph. Instead, [27] estimates the importance of candidate nodes in each node representation. Another line of research focuses on producing interpretable-by-design representations based on graph clustering [28], [29], which are conceptually analogous to community-preserving node embeddings [30].

Interpretability for link prediction. Our approach focuses on the interpretation of embedding dimensions according to the graph structural reconstruction task, and it is related to methods for the interpretability of embedding-based link prediction. For instance, ExplainE [31] quantifies the variation in the probability of a link when adding or removing neighboring edges. PaGE-Link [32] generates explanations as paths connecting a node pair, while ConPI [33] provides the most influential interactions computed with an attention mechanism over the contextual neighborhoods. Other relevant methods study the problem of explaining link prediction in knowledge graphs [34], [35]. We, on the other hand, aim to explain the node embedding itself by associating explanations with each of its dimensions.

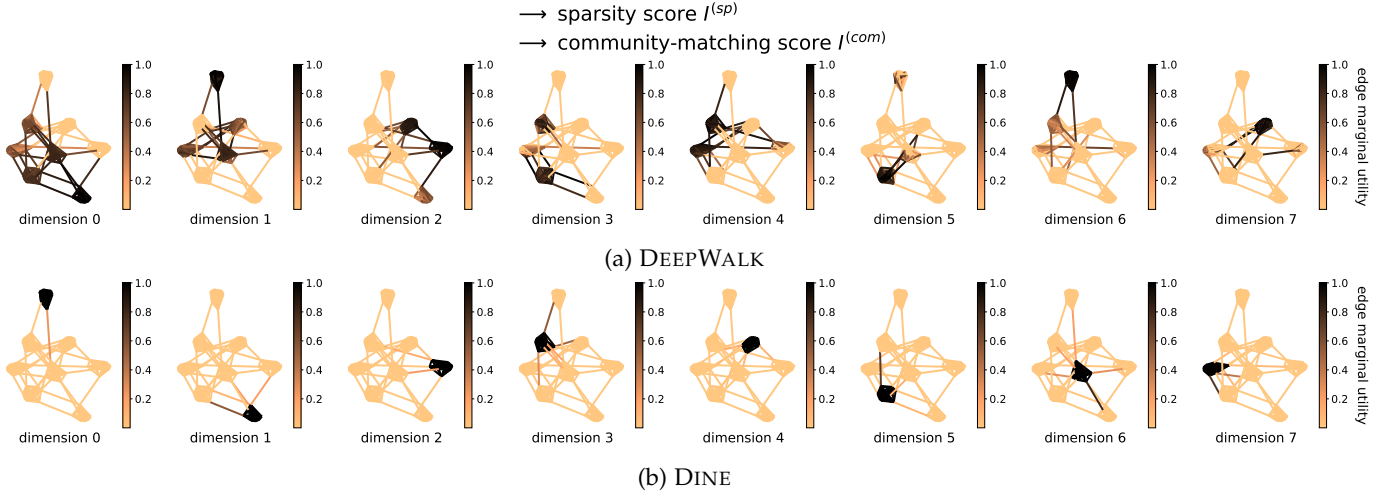


Fig. 1: Saliency plots with edge marginal utilities (normalized between 0 and 1) for 8-dimensional embeddings trained on a graph generated via stochastic block model [16], with 80 nodes divided into 8 cliques. In picture (a), from the left to the right, DEEPWALK dimensions are sorted by increasing their matching level with individual cliques, and with growing sparsity of the per-dimension subgraphs. In picture (b) our approach DINE is able to obtain interpretable dimensions both in terms of community-matching and sparsity.

Interpretability for word embeddings. Since many methods for graph representation learning are based on language models, techniques for interpreting the dimensions of word embeddings are also relevant for node embeddings. Previous literature in this area focuses on interpreting the dimensions of word embeddings based on semantic information [36], [37], or analyzing geometric properties of the embedding space [38], [39]. Several other studies also propose approaches to learn interpretable representations by design, where the goal is achieving *sparsity* [40]–[42]. However, due to the high popularity of some embedding approaches, post-processing techniques that are built upon these approaches have been often preferred rather than interpretable-by-design methods [43]–[45].

3 EXPLAINING NODE EMBEDDINGS

We start by formalizing the desired fundamental properties of a global explanation for node embeddings. Intuitively, as graph structure serves as the input for generating unsupervised node embeddings, we seek reliable explanations in terms of associations between model parameters and human-understandable units of the input graph.

Decomposability A global explanation should be able to refer to single parts of the model, and then explain these parts individually [46]. This is different from local instance-based explanation, where the focus is to interpret the result on single node predictions. In particular, a global explanation for node embeddings should be able to explain separately each dimension of the embedding space. To do so, in this work we extract interpretations in the form of important subgraphs \mathcal{G}_d that we identify as the “meaning”, or “explanation”, of a dimension d .

Comprehensibility An explanation should be human-understandable, in the sense that it relates to meaningful graph features [3] or discernible concepts [12]. With

subgraph-based explanations, such features can be seen as structural components that we identify with the *communities* of the graph. For instance in biological networks like protein-protein interaction networks, these subgraphs could be important pathways responsible for biological mechanisms associated with for example a protein function or disease progression. In other graphs such as social networks these subgraphs can be seen as communities. Communities are typically considered as one of the fundamental organizing principles in these graphs [15] justifying their choice to identify the meaning of representation dimensions.

Sparsity Explanations should be associated only with a minimal set of graph elements that sufficiently explain the learned parameters, ignoring the irrelevant ones [40], [41]. In our case, sparsity quantifies the spatial localization of an explanation subgraph

Having defined the desired properties, we next describe how to obtain such decomposable explanations for node embeddings. In Section 3.2 we propose new metrics to quantify both the comprehensibility and the sparsity of these explanations.

3.1 Decomposable explanations

Here we describe how we obtain global and decomposable explanations of node embeddings by extracting one explanation for every dimension of the latent space. Intuitively, given that embeddings are typically optimized for graph structure prediction, we aim to uncover the importance of individual dimensions in reconstructing the sub-structures of the graph. These substructures, consequently, will serve as explanations for individual dimensions. To extract the substructure explanations, we develop a utility function $\mu_d(\mathbf{u}, \mathbf{v})$ which quantifies the dimension’s contribution in reconstructing a single graph edge with an embedding decoder. In fact, the score returned by the decoder $\text{DEC}(\mathbf{u}, \mathbf{v})$

can be used to perform edge reconstruction, i.e. assessing the existence of edges (u, v) : the higher the score, the higher the likelihood of observing the link on the input graph.

Here we adopt a simple yet effective approach for attributing dimension importance based on feature removal [47], [48]. Specifically, we define the attribution score of a single dimension $d \in \mathcal{D}$ in the reconstruction of an edge (u, v) as:

$$\mu_d(\mathbf{u}, \mathbf{v}) = \Delta_{\mathcal{D}}(\mathbf{u}, \mathbf{v}) - \Delta_{\mathcal{D} \setminus \{d\}}(\mathbf{u}, \mathbf{v}), \quad (2)$$

where $\Delta_{\mathcal{S}} : \mathbb{R}^{|\mathcal{S}|} \times \mathbb{R}^{|\mathcal{S}|} \rightarrow \mathbb{R}$ quantifies the average edge scoring of dimensions in the subset $\mathcal{S} \subseteq \mathcal{D}$

$$\Delta_{\mathcal{S}}(\mathbf{u}, \mathbf{v}) = \frac{1}{|\mathcal{S}|} \sum_{d \in \mathcal{S}} \mathbf{u}_d \mathbf{v}_d. \quad (3)$$

Notably, we consider a product-based scoring function that is appropriate to work with popular methods such as DEEPWALK and NODE2VEC. For an individual edge, the function in Eq. (2) measures how much the average likelihood increases or decreases when removing dimension d from the whole set \mathcal{D} . From a game-theoretic point of view, the importance scores $\mu_d(\mathbf{u}, \mathbf{v})$ defined above is an example of *marginal utility*, which expresses the contribution of dimension d when it is added to the *coalitional set* $\mathcal{S} = \mathcal{D} \setminus \{d\}$. A more exhaustive computation takes into account the average marginal contribution according to any possible coalitional set $\mathcal{S} \subset \mathcal{D}$ and it is given by the Shapley value [49] score:

$$\phi_d(\mathbf{u}, \mathbf{v}) = \sum_{\mathcal{S} \subseteq \mathcal{D} \setminus \{d\}} \frac{\binom{|\mathcal{D}|-1}{|\mathcal{S}|}^{-1}}{|\mathcal{D}|} [\Delta_{\mathcal{S} \cup \{d\}}(\mathbf{u}, \mathbf{v}) - \Delta_{\mathcal{S}}(\mathbf{u}, \mathbf{v})], \quad (4)$$

where the difference $\Delta_{\mathcal{S} \cup \{d\}}(\mathbf{u}, \mathbf{v}) - \Delta_{\mathcal{S}}(\mathbf{u}, \mathbf{v})$ corresponds to the marginal utility of adding d to the dimensions' coalition $\mathcal{S} \subset \mathcal{D}$. Therefore, the importance score $\mu_d(\mathbf{u}, \mathbf{v})$ corresponds to the marginal utility given by Eq. (4) with respect to the maximal coalitions ($|\mathcal{S}| = |\mathcal{D}| - 1$).

Since the exact computation of (4) has exponential time complexity, several approximation methods have been proposed in the literature to address scalability issues [50], [51]. Additionally, most of the approximations assume independence among features [14], [50] and suffer from considering feature correlations [52]. Rather than introducing an approximation, the marginal utility adopted here helps to derive computationally feasible formulas: in fact, the computation of μ_d reduces the time complexity from the order of $2^{|\mathcal{D}|-1} |\mathcal{D}| |\mathcal{E}|$ to $|\mathcal{D}| |\mathcal{E}|$ when computed over all edges of the graph. Moreover, since mutual independence of features is not usually guaranteed for node embeddings, the simplification is due to express the effect of isolated dimensions disregarding possible feature correlations.

We use the importance scores defined in (2) to determine the explanation subgraphs formed by the edges that benefit most from the presence of a dimension d . Specifically, we identify the subgraph \mathcal{G}_d induced by links $\mathcal{E}_d = \{(u, v) \in \mathcal{E} : \mu_d(\mathbf{u}, \mathbf{v}) > 0\}$ with *positive* marginal utility as the explanation of dimension d . We restrict ourselves to positive payoffs because the main interest is to find those dimensions which are more effective in predicting a given edge, leaving for future work the analysis of the negative effects. In Figure 2

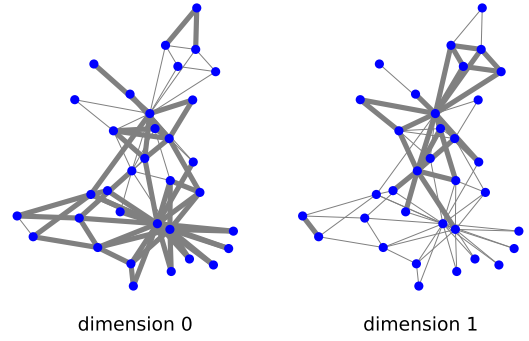


Fig. 2: Utility induced subgraphs for 2-dimensional DEEPWALK embeddings trained on KARATE-CLUB.

we highlight the explanation subgraphs in the KARATE-CLUB dataset for 2-dimensional DEEPWALK embeddings. We say that subgraphs depicted in Figure 2 are global explanations of DEEPWALK because they allow associating any model dimension with pieces of the data, and provide a global interpretation that is decomposed into per-dimension views.

3.2 Measuring comprehensibility and sparsity

Here we define metrics to quantify the quality of the extracted subgraph explanations. Specifically, we introduce two interpretability metrics to measure the comprehensibility and sparsity of the per-dimension induced subgraphs.

Community-aware metric. Let \mathcal{E}_d denote the set of edges in the explanation subgraph for dimension d . Given the information on important subgraphs for example pathways in case of biological networks or communities in social networks, we measure the relevance of explanation subgraphs to these communities/subgraphs using precision and recall scores. Let $\mathcal{P} = \{\mathcal{P}_1, \dots, \mathcal{P}_n\}$ denote the set of ground-truth link partitions/communities/subgraphs of the input graph. Later in the experiment section, we will also describe how to obtain such ground-truth subgraphs when these are not given. With the membership function $m : \mathcal{E} \rightarrow \mathcal{P}$, we first compute precision and recall metrics which measure the association strength of extracted explanation subgraphs with the given ground-truth important subgraphs/communities.

$$\text{precision}(\mathcal{E}_d, \mathcal{P}_i) = \frac{|\{(u, v) \in \mathcal{E}_d : m(u, v) = \mathcal{P}_i\}|}{|\mathcal{E}_d|} \quad (5)$$

$$\text{recall}(\mathcal{E}_d, \mathcal{P}_i) = \frac{|\{(u, v) \in \mathcal{E}_d : m(u, v) = \mathcal{P}_i\}|}{|\mathcal{P}_i|} \quad (6)$$

We then compute the interpretability score I_d as the maximum F1 score over all given ground-truth communities.

$$\hat{\mathcal{P}}_d = \operatorname{argmax}_{\mathcal{P}_i \in \mathcal{P}} \text{F1}(\mathcal{E}_d, \mathcal{P}_i); \quad I_d^{(com)} = \max_{\mathcal{P}_i \in \mathcal{P}} \text{F1}(\mathcal{E}_d, \mathcal{P}_i) \quad (7)$$

where F1-score is the harmonic mean between $\text{precision}(\mathcal{E}_d, \mathcal{P}_i)$ and $\text{recall}(\mathcal{E}_d, \mathcal{P}_i)$. Higher values of I_d indicate the dimension d is strongly associated with a single community. Global community-aware interpretability can be quantified with the average $I^{(com)} = \frac{1}{|\mathcal{D}|} \sum_{d \in \mathcal{D}} I_d^{(com)}$.

Sparsity-aware metric. In the absence of ground-truth community information, we can anyhow quantify in an

unsupervised manner whether dimensions can highlight structure-relevant subgraphs. In particular, without any cognition on community structure, it is highly preferable that interpretable directions of the embedding space are associated with a minimal set of significant edges. Inspired by explanation masks in graph neural networks [53], we formulate its calculation using Shannon entropy [54]:

$$I_d^{(sp)} = -\frac{1}{\log |\mathcal{E}|} \sum_{(u,v) \in \mathcal{E}} \left(\frac{[(u,v) \in \mathcal{E}_d]}{z_d} \right) \log \left(\frac{[(u,v) \in \mathcal{E}_d]}{z_d} \right) \quad (8)$$

where the function $[*]$ returns 1 if the proposition inside is true (and 0 otherwise), and $z_d = \sum_{(u,v) \in \mathcal{E}} [(u,v) \in \mathcal{E}_d]$ is a normalization for the correct computation of the Shannon entropy. Lower values indicate that embedding dimensions are associated with smaller-sized subgraphs. Global sparsity-aware interpretability can be quantified with the average $I^{(sp)} = \frac{1}{|\mathcal{D}|} \sum_{d \in \mathcal{D}} I_d^{(sp)}$.

4 OUR APPROACH: DIMENSION-BASED INTERPRETABLE NODE EMBEDDING

In previous sections, we proposed the utility-induced subgraphs as explanations to interpret node embedding dimensions. Unsurprisingly, as we show in Figure 1(a) for DEEPWALK, typically it is difficult to map utility-induced subgraphs to interpretable graph units, mainly because these methods are trained with the unique goal of maximizing reconstruction performance. Filling this gap, we introduce *Dimension-based Interpretable Node Embedding* (DINE), a novel method to improve the interpretability of already trained node embeddings by retrofitting the induced subgraphs which affect interpretation metrics (§3.2).

We design such retrofit task with an autoencoder architecture, trained to reconstruct embedding vectors in the input [55]. By encoding the input node representations into a hidden feature space, the autoencoder can be regularized in order to promote the learning of interpretable dimensions. Despite the many existing regularizations already used to obtain interpretable embeddings, such as non-negativity [42], [56] or sparsity [41], [43], in this work we employ *orthogonality* regularizers [57]–[59] to achieve the purpose. Orthogonality is closely related with *disentanglement* [60], [61], which is a key concept implemented in several methods for decoupling correlations between latent dimensions [62], [63], with the results of learning more compact representations whose feature dimensions are associated with independent facets of data.

We argue improving dimension-based orthogonality is more effective for several reasons:

- *Distinct features*: If two dimensions are orthogonal, it means that they are independent of each other and do not share any latent factor. Therefore, each dimension provides unique information which can be interpreted as representing a distinct characteristic of the data.
- *Separation of concepts*: Orthogonal dimensions in the embedding space can represent independent concepts. For example, in the context of word embeddings, the concept of "gender" might be captured along one dimension, while the concept of "age" might be captured along

another. This helps us to easily separate and understand these different features of the data.

- *Removing redundancy*: Orthogonality implies no redundancy. If two dimensions are not orthogonal, then they project onto each other to some extent, meaning there's some shared information. This shared information could be interpreted as redundancy. By ensuring orthogonality, we ensure that each latent direction provides new, unique information.
- *Clear interpretation of distances*: In an orthogonal space, distances directly correlate with dissimilarity. For instance, two orthogonal word embeddings would likely represent words with very different meanings or features, while vectors closer together would represent more similar words.

Contrary to previous works [59] that enforce orthogonality of neural weights, here we employ orthogonalization of the edge reconstruction patterns that directly affect per-dimension utility subgraphs. In this way, we obtain node embeddings whose interpretability is optimized according to metrics introduced in previous section. In the next, we first show how we can rephrase the utility optimization in an effective way to be easily handled, and how the method is implemented.

4.1 Optimization of Marginal Utilities

DINE aims to learn an opportune mapping $h : \mathbb{R}^D \rightarrow \mathbb{R}^K$, in such a way that per-dimension subgraphs are highly interpretable in terms of decomposability, comprehensibility and sparsity of explanations. We use both \mathbf{v}^* and $h(\mathbf{v})$ to indicate the embedding vectors of node $v \in \mathcal{V}$ mapped with the embedding function h , and collected into the matrix $\mathbf{H} \in \mathbb{R}^{K \times |\mathcal{V}|}$. We also refer to K as the cardinality of the set containing the enumerated dimensions of the new space $\mathcal{K} = \{1, \dots, K\}$.

Since subgraphs are the results of positive marginal utilities $\mu_d(\mathbf{u}^*, \mathbf{v}^*)$, we are interested in optimizing the utility measures as a function of the new embedding parameters defined by h . In the following paragraphs we show that, assuming the new embedding space to be the unit-size hypercube $[0, 1]^K \subset \mathbb{R}^K$, together with sufficiently high embedding dimensionality, we can simplify the optimization of the utility measure. In fact, in the following theorem we show that for a given edge, the interpretability (utility) measure for a dimension can be approximated using a single dot product over the embedding pair.

Theorem. *Let be $h : \mathbb{R}^D \rightarrow [0, 1]^K$ the mapping from an embedding encoder of $\mathcal{G} = (\mathcal{V}, \mathcal{E})$ and the K -dimensional hypercube. For high dimensionality K , the per-dimension utility score for edge $(u, v) \in \mathcal{E}$, $\mu_d(\mathbf{u}^*, \mathbf{v}^*)$, can be expressed as:*

$$\mu_d(\mathbf{u}^*, \mathbf{v}^*) + \mathcal{O}\left(\frac{1}{K^2}\right) = \frac{\mathbf{u}_d^* \mathbf{v}_d^*}{K}$$

Proof. We start writing the formula for $\mu_d(\mathbf{u}^*, \mathbf{v}^*)$:

$$\mu_d(\mathbf{u}^*, \mathbf{v}^*) = \frac{1}{K} \sum_{q \in \mathcal{K}} \mathbf{u}_q^* \mathbf{v}_q^* - \frac{1}{K-1} \sum_{q \in \mathcal{K} \setminus \{d\}} \mathbf{u}_q^* \mathbf{v}_q^*$$

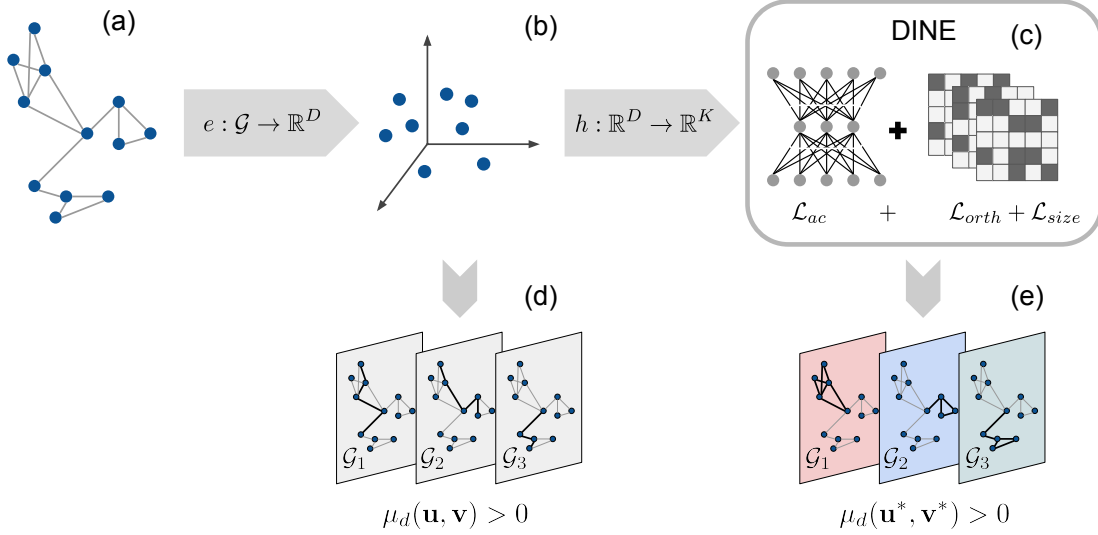


Fig. 3: Schematic view of our methodology. Starting from a graph (a), we consider a given embedding representation (b), to which we apply the method DINE (c). Explanations are given in the form of per-dimension subgraphs, both for the starting embedding (d) and the DINE embedding (e).

Using the expression $\sum_{q \in \mathcal{K}} u_q^* v_q^* = \mathbf{u}^* \cdot \mathbf{v}^* = u_d^* v_d^* + \sum_{q \in \mathcal{K} \setminus \{d\}} u_q^* v_q^*$, we find that:

$$\begin{aligned} \mu_d(\mathbf{u}^*, \mathbf{v}^*) &= \frac{1}{K} u_d^* v_d^* - \left(\frac{1}{K-1} - \frac{1}{K} \right) \sum_{q \in \mathcal{K} \setminus \{d\}} u_q^* v_q^* \\ &= \frac{1}{K} u_d^* v_d^* - \frac{1}{K} \left(\frac{1}{1 - \frac{1}{K}} - 1 \right) (\mathbf{u}^* \cdot \mathbf{v}^* - u_d^* v_d^*) \end{aligned}$$

Ignoring the case of 1-dimensional embeddings, $K > 1$ and $0 < \frac{1}{K} < 1$, then the expression in the first parenthesis can be rewritten using the geometric series:

$$\frac{1}{1 - \frac{1}{K}} - 1 = \sum_{l=0}^{\infty} \frac{1}{K^l} - 1 = \frac{1}{K} + \mathcal{O}\left(\frac{1}{K^2}\right)$$

replacing the formula with this last result, we have:

$$\begin{aligned} K \cdot \mu_d(\mathbf{u}^*, \mathbf{v}^*) &= u_d^* v_d^* - \left(\frac{1}{K} + \mathcal{O}\left(\frac{1}{K^2}\right) \right) (\mathbf{u}^* \cdot \mathbf{v}^* - u_d^* v_d^*) \\ &= u_d^* v_d^* \left(1 + \frac{1}{K} + \mathcal{O}\left(\frac{1}{K^2}\right) \right) - \mathbf{u}^* \cdot \mathbf{v}^* \left(\frac{1}{K} + \mathcal{O}\left(\frac{1}{K^2}\right) \right) \\ &= (u_d^* v_d^* - \frac{1}{K} \mathbf{u}^* \cdot \mathbf{v}^*) \left(1 + \frac{1}{K} + \mathcal{O}\left(\frac{1}{K^2}\right) \right) \end{aligned}$$

In the case of the function h , we have $u_d^* \cdot v_d^* \in [0, 1]$ and so $\mathbf{u}^* \cdot \mathbf{v}^* = \alpha_{uv} K$, where $0 < \alpha_{uv} < 1$. With sufficient high dimensionality K , we can assume that values $u_d^* \cdot v_d^*$ are independent from the dimensionality K , then $\alpha_{uv} \propto \frac{1}{K}$. Therefore, neglecting infinitesimal terms in parenthesis we obtain $\mu_d(\mathbf{u}^*, \mathbf{v}^*) + \frac{\alpha_{uv}}{K} + \mathcal{O}\left(\frac{1}{K^2}\right) = \mu_d(\mathbf{u}^*, \mathbf{v}^*) + \mathcal{O}\left(\frac{1}{K^2}\right) \approx \frac{u_d^* v_d^*}{K}$. \square

We define $\frac{u_d^* v_d^*}{K}$ as the entries $m_d^*(u, v)$ of K continuous-valued graph masks $\{\mathbf{M}_d \in \mathbb{R}^{|\mathcal{V}| \times |\mathcal{V}|}\}_{d \in \mathcal{K}}$, that can be easily computed as the outer products of the rows of \mathbf{H} , namely $m_d^*(u, v) = (\mathbf{H}_{d,:} \otimes \mathbf{H}_{d,:})_{uv}$.

The equation $\mu_d(\mathbf{u}^*, \mathbf{v}^*) + \mathcal{O}\left(\frac{1}{K^2}\right) \approx \frac{u_d^* v_d^*}{K} \equiv m_d^*(u, v)$ tells that the quantities $m_d^*(u, v)$ and $\mu_d(\mathbf{u}^*, \mathbf{v}^*)$ differ by a negligible term $\mathcal{O}\left(\frac{1}{K^2}\right)$. Consequently, we can optimize the quantities $m_d^*(u, v)$ that are computed from individual products. Graph masks have the role of highlighting the structure-relevant edges for any direction in the K -dimensional learned space.

4.2 Method Implementation

We now describe the retro-fitting optimization task and identify the key design choices which allow obtaining more interpretable induced subgraphs, and whose effectiveness is shown in the experiments section. Please refer to Figure 3 for a schematic diagram of our approach.

We implemented h as the latent projection of a single-layer autoencoder, namely $h(\mathbf{v}) = \sigma(\mathbf{W}^{(0)} \mathbf{v} + \mathbf{b}^{(0)})$, which returns $\tilde{\mathbf{v}} = \mathbf{W}^{(1)} h(\mathbf{v}) + \mathbf{b}^{(1)}$ as output. The hidden layer matrix of the autoencoder, $\mathbf{H} \in \mathbb{R}^{K \times |\mathcal{V}|}$, collects the components $H_{d,v} = h_d(\mathbf{v}) \in [0, 1]$ of the interpretable embedding vectors that we aim to learn.

We add regularization constraints on the hidden embedding matrix \mathbf{H} while training the autoencoder, in order to learn optimal graph masks. Specifically, we minimize the following loss:

$$\mathcal{L} = \mathcal{L}_{ac}(\mathbf{X}, \tilde{\mathbf{X}}) + \sum \mathcal{L}_{reg}(\mathbf{H}) \quad (9)$$

where $\mathcal{L}_{ac}(\mathbf{X}, \tilde{\mathbf{X}}) = \text{MSE}(\mathbf{X}, \tilde{\mathbf{X}}) = \frac{1}{|\mathcal{V}|} \sum_{v \in \mathcal{V}} \|\mathbf{X}_{:,v} - \tilde{\mathbf{X}}_{:,v}\|^2$ is the mean squared error between the input and output embedding matrices $\mathbf{X}, \tilde{\mathbf{X}} \in \mathbb{R}^{D \times |\mathcal{V}|}$. We jointly optimise masks matrices $\{\mathbf{M}_d \in \mathbb{R}^{|\mathcal{V}| \times |\mathcal{V}|}\}_{d \in \mathcal{K}}$, computed from hidden layer parameters \mathbf{H} , and the autoencoder parameters $\{\mathbf{W}^{(0)} \in \mathbb{R}^{K \times D}, \mathbf{W}^{(1)} \in \mathbb{R}^{D \times K}, \mathbf{b}^{(0)} \in \mathbb{R}^K, \mathbf{b}^{(1)} \in \mathbb{R}^D\}$. We determined the following regularization terms as optimal for promoting interpretable dimensions:

- Induced subgraphs might have minimal overlaps between each other in order to be interpreted as communities.

Inspired by graph clustering [64], we squeeze embedding mask matrices into one partition matrix $\mathbf{P} \in \mathbb{R}^{K \times |\mathcal{V}|}$, with entries $P_{d,v} = \sum_{u \in \mathcal{V}} m_d^*(u, v)$, computed by aggregating edge reconstruction scores with the same target node¹. In order to encourage relevant subgraphs to be incorporated into different embedding axes, we optimize the following *Orthogonality Loss*:

$$\mathcal{L}_{orth} = \text{MSE}\left(\frac{\mathbf{P}\mathbf{P}^T}{\|\mathbf{P}\mathbf{P}^T\|_F}, \frac{\mathbf{1}_K}{\|\mathbf{1}_K\|_F}\right) \quad (10)$$

The use of node-based partition is due to scalability reasons: the entries of the partition matrix $P_{d,v} = \sum_u m_d^*(u, v) \propto h_d(\mathbf{v})[\sum_u h_d(\mathbf{u})]$ can be computed avoiding the explicit calculation and caching of $\mathcal{O}(K \times |\mathcal{V}| \times |\mathcal{V}|)$ parameter for graph masks, reducing the complexity to $\mathcal{O}(K \times |\mathcal{V}|)$.

- In order to avoid degenerate solutions due to the orthogonality constraint, e.g. all relevant subgraphs reconstructed in the same dimension, we enforce the size of every mask $s_d = \sum_{u,v} m_d^*(u, v)$ to be non-zero. This constraint is accomplished by maximizing the entropy of the size variables $\{s_d\}_{d \in \mathcal{K}}$, opportunely normalized, or equivalently minimizing the *Size Loss*:

$$\mathcal{L}_{size} = \log |\mathcal{K}| + \sum_{d \in \mathcal{K}} \frac{s_d}{\sum_{q \in \mathcal{K}} s_q} \log \frac{s_d}{\sum_{q \in \mathcal{K}} s_q} \quad (11)$$

The full objective loss is given by:

$$\mathcal{L} = \mathcal{L}_{ac}(\mathbf{X}, \tilde{\mathbf{X}}) + \mathcal{L}_{orth}(\mathbf{H}) + \mathcal{L}_{size}(\mathbf{H}) \quad (12)$$

5 EXPERIMENTS

In this section, we present the results of our study on the DINE model from different perspectives. The main objective is to address the following research questions:

- RQ1** How does the interpretability of DINE compare to those of standard embedding techniques?
- RQ2** How well does DINE perform in the link prediction task?
- RQ3** Is DINE suitable for practical use, particularly in scenarios requiring scalability?

In the following sections, we describe the data, models, and tasks used in the comparison to address our research questions.

5.1 Data and Models

TABLE 1: Summary statistics about real-world graph data. In order: number of nodes $|\mathcal{V}|$, number of edges $|\mathcal{E}|$, number of extracted communities $|\mathcal{C}|$ with Louvain method.

Dataset	$ \mathcal{V} $	$ \mathcal{E} $	$ \mathcal{C} $
CORA	2,485	5,069	28
CITeseer	2,110	3,668	35
PUBMED	19,717	44,324	38
BLOG	5,196	171,743	10
FLICKR	7,575	239,738	9
WIKI	2,357	11,592	17

1. Aggregating over the source node would give the same result since we work with undirected graphs and $M_d(u, v) = M_d(v, u)$.

We present our results on a variety of benchmark datasets used in prior work [65]: three citation networks (CORA, CITESEER and PUBMED), two social networks (BLOG and FLICKR), and a web pages network (WIKI). Despite their original format, we restrict our analysis to the large connected component of any graph, considered unweighted and undirected.

As described in Section 3.2, we rely on *ground-truth link partitions* for interpretability metrics based on community structure. Many empirical graphs have node metadata that can be used for node-to-community mapping. However, the use of metadata as structure-aware labels has recently been criticized by previous works [66], [67]. Instead, we use community detection to discover partition labels. We avoid computationally expensive and overlapping community detection methods [68]–[71] and use the arguably intuitive and simpler Louvain detection method [72] to derive edge labels based on node-level graph communities. Specifically, we ran Louvain detection method [72] to extract the node-level communities $\mathcal{C} = \{\mathcal{C}_1, \dots, \mathcal{C}_m\}$ and we assign partition label for a given edge (u, v) the set $\{c(u), c(v)\}$, where $c: \mathcal{V} \rightarrow \mathcal{C}$ is the node-level community membership function. We report datasets statistics in Table 1.

We use the following baseline methods:

- DEEPWALK [17], skip-gram based model that computes node embeddings from random walks co-occurrence statistics. We train NODE2VEC² for 5 epochs with the following parameters: p=1, q=1, walk_length=10, num_walks=20, window_size=5.
- GAE [22], neural network model with a GCN encoder trained on adjacency matrix reconstruction. The model³ is trained for 200 iterations using Adam optimizer and learning rate of 0.01 as described in the main paper. The GCN hidden layer size is taken double the output size.
- GEMSEC [29], a variation of DEEPWALK which jointly learns node embeddings and node clusters. We train the model⁴ with the same configuration as DEEPWALK, plus the number of clusters fixed equal to the number of dimensions.
- SPINE [43], a post-processing technique based on *k* – *sparse* denoising autoencoder to generate sparse embeddings. We train the original model⁵ for 2000 iterations with sparsity 0.15 and learning rate 0.1.

DINE is trained for 2000 iterations, and learning rate of 0.1, with DEEPWALK and GAE embeddings, to show the capability of DINE in handling models with different inductive biases. With SPINE we post-process DEEPWALK vectors for a dedicated analysis.

5.2 Tasks Description

For answering **RQ1**, we measure the interpretability of DINE in comparison to our baseline methods. To do so, we compute for any embedding dimension interpretability scores that we have defined in §3.2. Instead of averaging over all dimensions for comparing the models, we focus on a subset of effective dimensions \mathcal{D}_{eff} that encode the majority

2. <https://github.com/eliorc/node2vec>

3. <https://github.com/zfjsail/gae-pytorch>

4. <https://github.com/benedekrozemberczki/karateclub>

5. <https://github.com/harsh19/SPINE>

TABLE 2: Community-aware scores for interpretability evaluation of different embedding methods. For each dataset, we highlight the best (highest) score.

	CITESEER	PUBMED	BLOG	FLICKR	WIKI
DEEPWALK	0.433 (± 0.014)	0.422 (± 0.011)	0.432 (± 0.007)	0.499 (± 0.105)	0.445 (± 0.025)
GAE	0.420 (± 0.010)	0.487 (± 0.019)	0.496 (± 0.006)	0.625 (± 0.021)	0.460 (± 0.014)
GEMSEC	0.446 (± 0.014)	0.431 (± 0.009)	0.392 (± 0.030)	0.421 (± 0.022)	0.454 (± 0.002)
DEEPWALK+DINE	0.641 (± 0.027)	0.605 (± 0.027)	0.590 (± 0.023)	0.657 (± 0.014)	0.652 (± 0.010)
GAE+DINE	0.526 (± 0.008)	0.593 (± 0.011)	0.600 (± 0.008)	0.595 (± 0.013)	0.631 (± 0.017)
DEEPWALK	0.491 (± 0.016)	0.457 (± 0.006)	0.483 (± 0.009)	0.469 (± 0.018)	0.496 (± 0.009)
DEEPWALK+SPINE	0.543 (± 0.060)	0.608 (± 0.037)	0.632 (± 0.082)	0.703 (± 0.001)	0.611 (± 0.015)
DEEPWALK+DINE	0.641 (± 0.027)	0.605 (± 0.027)	0.590 (± 0.023)	0.657 (± 0.014)	0.652 (± 0.010)

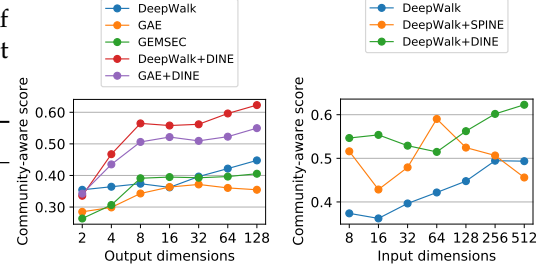


Fig. 4: Community-aware scores for CORA (higher is better). On the left, we compare the community-aware scores of different dense embedding methods when varying the number of output dimensions and choosing the best score among models over different number of input dimensions. On the right, we compare the scores of DEEPWALK and SPINE when varying the number of input dimensions and choosing the best score among models over different number of output dimensions.

TABLE 3: Sparsity-aware scores for interpretability evaluation of different embedding methods. For each dataset, we highlight the best (lowest) score.

	CITESEER	PUBMED	BLOG	FLICKR	WIKI
DEEPWALK	0.778 (± 0.006)	0.849 (± 0.001)	0.865 (± 0.002)	0.874 (± 0.004)	0.820 (± 0.003)
GAE	0.825 (± 0.004)	0.851 (± 0.005)	0.871 (± 0.009)	0.785 (± 0.001)	0.844 (± 0.002)
GEMSEC	0.817 (± 0.003)	0.865 (± 0.002)	0.911 (± 0.003)	0.916 (± 0.002)	0.846 (± 0.004)
DEEPWALK+DINE	0.630 (± 0.015)	0.684 (± 0.242)	0.749 (± 0.006)	0.372 (± 0.069)	0.688 (± 0.003)
GAE+DINE	0.728 (± 0.009)	0.805 (± 0.003)	0.820 (± 0.012)	0.711 (± 0.021)	0.756 (± 0.003)
DEEPWALK	0.755 (± 0.003)	0.836 (± 0.001)	0.840 (± 0.001)	0.874 (± 0.004)	0.796 (± 0.004)
DEEPWALK+SPINE	0.703 (± 0.025)	0.741 (± 0.033)	0.610 (± 0.089)	0.729 (± 0.125)	0.529 (± 0.097)
DEEPWALK+DINE	0.630 (± 0.015)	0.748 (± 0.008)	0.749 (± 0.006)	0.681 (± 0.060)	0.688 (± 0.003)

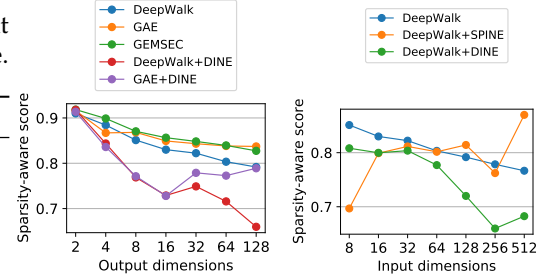


Fig. 5: Sparsity-aware scores for CORA (lower is better). On the left, we compare the sparsity-aware scores of different dense embedding methods when varying the number of output dimensions and choosing the best score among models with a different number of input dimensions. On the right, we compare the scores of DEEPWALK and SPINE when varying the number of input dimensions and choosing the best score among models with a different number of output dimensions.

of edge information, to avoid potential noise from the less important dimensions. Specifically, after computing $I_d^{(com)}$ or $I_d^{(sp)}$, we select the top-ranked dimensions that cumulatively contribute to the reconstruction of at least 90% of the graph edges, i.e., $|\bigcup_{d \in \mathcal{D}_{eff}} \mathcal{E}_d| = 90\%|\mathcal{E}|$. Thus we compute global scores as $I_{eff}^{(com|sp)} = \frac{1}{|\mathcal{D}_{eff}|} \sum_{d \in \mathcal{D}_{eff}} I_d^{(com|sp)}$. For answering **RQ2**, we measure the link prediction performance of DINE in comparison to our baseline methods. To do so, before training every method, we randomly remove 10% of the edges that are used as positive examples for the link prediction task on one hand. On the other hand, we also sample the same number of node pairs from the set of non-existing links as negative examples. The task consists in ranking the collected node pairs with the scoring function Δ and evaluating the classification performance with the ROC-AUC score.

5.3 Results

In our experiments, all methods, with the exception of SPINE, are trained to produce embedding vectors with dimensions in the set $\{2, 4, 8, 16, 32, 64, 128\}$, referred to as *output dimensions*. On the other hand, the *input dimensions* for DEEPWALK and GAE vectors used for training DINE and SPINE (only DEEPWALK for the latter), taken from the set $\{8, 16, 32, 64, 128, 256, 512\}$, define the *dimensionality* of the input vectors. For SPINE, due to the presence of the overcomplete layer, we chose output dimensions to be multiples of the input dimensions, i.e. between $\times 1$ and $\times 8$.

In our comparison, we evaluated DINE against both dense and sparse methods. For the comparison with dense methods, DINE was trained using DEEPWALK and GAE vectors, with performance reported across different output dimensions. To compare with sparse methods, both SPINE and DINE were trained using DEEPWALK vectors, with

TABLE 4: ROC-AUC scores for link prediction performance of different embedding methods. For each dataset, we show in boldface letters the best score, and we highlight with gray background other methods that reach at least 95% of the best model score.

	CITESEER	PUBMED	BLOG	FLICKR	WIKI
DEEPWALK	0.945 (± 0.007)	0.964 (± 0.002)	0.756 (± 0.001)	0.656 (± 0.001)	0.848 (± 0.003)
GAE	0.952 (± 0.006)	0.958 (± 0.002)	0.869 (± 0.003)	0.894 (± 0.004)	0.942 (± 0.002)
GEMSEC	0.942 (± 0.007)	0.951 (± 0.003)	0.794 (± 0.002)	0.670 (± 0.003)	0.905 (± 0.004)
DEEPWALK+DINE	0.947 (± 0.010)	0.933 (± 0.012)	0.747 (± 0.006)	0.759 (± 0.009)	0.905 (± 0.004)
GAE+DINE	0.920 (± 0.009)	0.961 (± 0.001)	0.820 (± 0.010)	0.911 (± 0.003)	0.942 (± 0.004)
DEEPWALK	0.949 (± 0.008)	0.965 (± 0.001)	0.758 (± 0.001)	0.667 (± 0.002)	0.848 (± 0.002)
DEEPWALK+SPINE	0.897 (± 0.021)	0.902 (± 0.006)	0.673 (± 0.014)	0.632 (± 0.035)	0.816 (± 0.014)
DEEPWALK+DINE	0.947 (± 0.010)	0.933 (± 0.012)	0.747 (± 0.006)	0.759 (± 0.009)	0.905 (± 0.004)

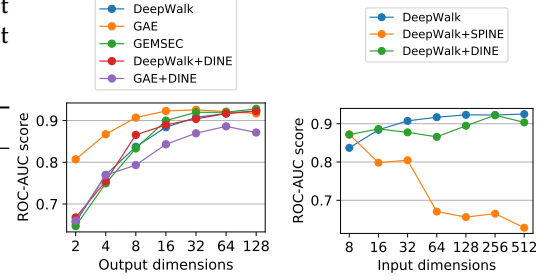


Fig. 6: ROC-AUC scores for link prediction in CORA. On the left, we compare the ROC-AUC scores of different dense embedding methods when varying the number of output dimensions and choosing the best score among models with a different number of input dimensions. On the right, we compare the scores of DEEPWALK and SPINE when varying the number of input dimensions and choosing the best score among models with a different number of output dimensions.

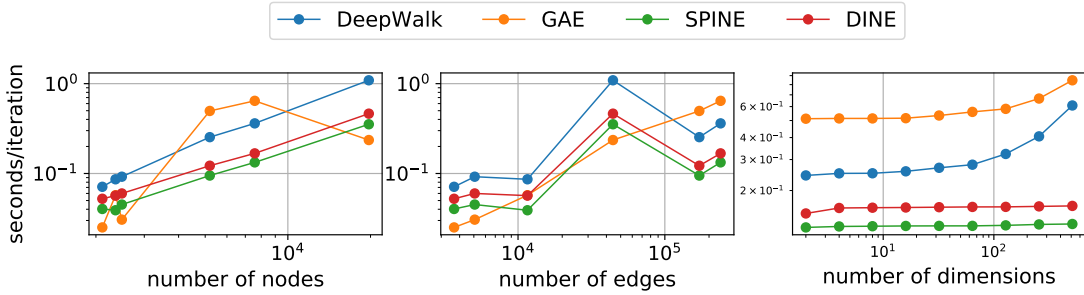


Fig. 7: Normalized execution times for different embedding methods when trained on multiple datasets. In the left, we compare running times while varying the number of nodes with 128-dim output embeddings; in the center, we compare running times while varying the number of edges with 128-dim output embeddings; in the right, we compare running times while varying the number of embedding dimensions in FLICKR dataset.

their performance reported across different input DEEPWALK dimensions. The results for dense and sparse embeddings are reported respectively at the top and at the bottom of each table, with average evaluation score and standard deviation computed over 5 separate training runs. Additional figures are reported in the Appendix with all the results not shown in the main paper.

Interpretability (RQ1). Best scores for our interpretability metric $I_{eff}^{(com)}$ and $I_{eff}^{(sp)}$ are reported in Tables 2 and 3 respectively for all the datasets, with detailed plots in Figures 4 and 5 for CORA. We notice that the combination DEEPWALK+DINE performs well with respect to dense embeddings in almost every dataset where their vector dimensions are sparse and are grounded in the community structure. The model GAE+DINE is less interpretable than DEEPWALK+DINE, but still more interpretable than the other dense baselines. Both DINE and SPINE models trained on DEEPWALK vectors demonstrate good interpretability, obtaining the best scores in half of the datasets each. Our results confirm the well-known property of vector sparsity improving the interpretability of representations [73].

Additionally, we observe that both interpretability metrics improve as the embedding dimensions increase in the CORA dataset (Figures 4 and 5). This is true also in the other datasets shown in the Appendix, providing important guidance for choosing the appropriate embedding size in real-world applications.

Link prediction (RQ2). ROC-AUC scores are documented in Table 4 for all datasets, with a detailed illustration for CORA in Figure 6. The results show that in citation networks, all models, including DINE retrofitted embeddings, perform similarly to the optimal results obtained from dense embeddings. The implication of this result is that we do not have to trade task performance with increased interpretability. In other datasets, the best scores are obtained by GAE and GAE+DINE. In fact, when comparing sparse embeddings, DEEPWALK+DINE **consistently outperforms** DEEPWALK+SPINE, with comparable or even superior results (in the case of FLICKR and WIKI) to DEEPWALK. Interestingly, our results in Figure 6 also demonstrate that SPINE’s performance decreases with increasing input dimensions, unlike the other methods.

Scalability (RQ3). The training times for various methods are presented in Figure 7, with the intervals normalized relative to the number of iterations/epochs. For DEEPWALK, the intervals are further divided with respect to the `num_walks` parameter to remove the dependence on the number of walks per node. Experimental results on the scalability suggest that it is possible to increase the interpretability of node representations without requiring significant computational costs. The left panel shows that the runtimes for DEEPWALK, SPINE, and DINE increase with the number of nodes, while the center panel demonstrates that the execution time for GAE increases with the number of edges. Additionally, DINE has slightly longer training times compared to SPINE, but both are faster than DEEPWALK. The right panel indicates that the training time for SPINE and DINE has a weak dependence on the number of embedding dimensions, while this dependence is more pronounced in GAE and DEEPWALK.

6 CONCLUSION AND FUTURE WORK

In this work, we presented a framework for constructing global explanations for node embeddings. We explain each embedding dimension using the important substructures of the input graph. To construct these explanations we developed a new *model-agnostic* utility measure which computes the contributions of each dimension to predict the graph structure. Our explanations follow the desired properties of decomposability, comprehensibility and sparsity.

With the goal of maximizing these properties, we proposed and developed DINE, an auto-encoder framework to enhance the interpretability of existing node embeddings. In short, DINE captures the structural properties encoded in an input embedding and optimizes a set of graph masks in order to promote orthogonality and sparsity of predicted substructures. Our comprehensive experimental study supports our claims that DINE improves embedding comprehensibility over standard node embedding techniques, without compromising the task performance. DINE is also preferable to the sparse method SPINE due to its better achievements in link prediction. DINE scales well with respect to the input graph size, being suitable to be used in graphs with high edge density. Since the computation of the exact utility measure has exponential complexity as is usually the case for Shapley-based measures, the presented utility measure shares limitations common to other approximation strategies suggested in the literature. In particular, the approximation deteriorates under high interdependence among embedding features [52]. Nevertheless, the encouraging results from our experiments support the effectiveness of this approach.

These contributions open multiple avenues for future work. Specifically, our approach can be extended to constructing interpretable node embeddings whose dimensions are aware of multi-scale subgraph structures [74] inherent in many real-world graphs [75]. DINE can also be used as a plug-in architecture to facilitate interpretable learning in various graph neural network encoders [22].

ACKNOWLEDGMENTS

S. Piaggese acknowledges partial support from the European Community program under the funding schemes: G.A.

n.871042, “SoBigData++: European Integrated Infrastructure for Social Mining and Big Data Analytics”; G.A. 834756 “XAI: Science and technology for the eXplanation of AI decision making”. The funder had no role in study design, data collection and analysis, decision to publish, or preparation of the manuscript.

REFERENCES

- [1] W. L. Hamilton, “Graph representation learning,” *Synthesis Lectures on Artificial Intelligence and Machine Learning*, vol. 14, no. 3, pp. 1–159, 2020.
- [2] N. Liu, X. Huang, J. Li, and X. Hu, “On interpretation of network embedding via taxonomy induction,” in *Proceedings of the 24th ACM SIGKDD International Conference on Knowledge Discovery & Data Mining*, pp. 1812–1820, 2018.
- [3] A. Dalmia, G. J., and M. Gupta, “Towards Interpretation of Node Embeddings,” in *Companion of the The Web Conference 2018 on The Web Conference 2018 - WWW '18*, (Lyon, France), pp. 945–952, ACM Press, 2018.
- [4] A. Gogoglou, C. B. Bruss, and K. E. Hines, “On the Interpretability and Evaluation of Graph Representation Learning,” *NeurIPS workshop on Graph Representation Learning*, 2019.
- [5] C. V. Cannistraci, G. Alanis-Lobato, and T. Ravasi, “From link-prediction in brain connectomes and protein interactomes to the local-community-paradigm in complex networks,” *Scientific reports*, vol. 3, no. 1, p. 1613, 2013.
- [6] X. Yue, Z. Wang, J. Huang, S. Parthasarathy, S. Moosavinasab, Y. Huang, S. M. Lin, W. Zhang, P. Zhang, and H. Sun, “Graph embedding on biomedical networks: methods, applications and evaluations,” *Bioinformatics*, vol. 36, pp. 1241–1251, 10 2019.
- [7] T. N. Dong, J. Schrader, S. Mücke, and M. Khosla, “A message passing framework with multiple data integration for mirna-disease association prediction,” *Scientific Reports*, vol. 12, 2022.
- [8] Z. Ying, D. Bourgeois, J. You, M. Zitnik, and J. Leskovec, “Gnnexplainer: Generating explanations for graph neural networks,” *Advances in neural information processing systems*, vol. 32, 2019.
- [9] T. Funke, M. Khosla, M. Rathee, and A. Anand, “Zorro: Valid, sparse, and stable explanations in graph neural networks,” *IEEE Transactions on Knowledge and Data Engineering*, 2022.
- [10] M. Vu and M. T. Thai, “Pgm-explainer: Probabilistic graphical model explanations for graph neural networks,” *Advances in neural information processing systems*, vol. 33, pp. 12225–12235, 2020.
- [11] C. T. Duong, Q. V. H. Nguyen, and K. Aberer, “Interpretable node embeddings with mincut loss,” in *Learning and Reasoning with Graph-Structured Representations Workshop-ICML*, 2019.
- [12] M. Idahl, M. Khosla, and A. Anand, “Finding interpretable concept spaces in node embeddings using knowledge bases,” in *Machine Learning and Knowledge Discovery in Databases: International Workshops of ECML PKDD 2019, Würzburg, Germany, September 16–20, 2019, Proceedings, Part I*, pp. 229–240, Springer, 2020.
- [13] M. T. Ribeiro, S. Singh, and C. Guestrin, “‘why should i trust you?’ explaining the predictions of any classifier,” in *Proceedings of the 22nd ACM SIGKDD international conference on knowledge discovery and data mining*, pp. 1135–1144, 2016.
- [14] S. M. Lundberg and S.-I. Lee, “A unified approach to interpreting model predictions,” *Advances in neural information processing systems*, vol. 30, 2017.
- [15] M. Girvan and M. E. Newman, “Community structure in social and biological networks,” *Proceedings of the national academy of sciences*, vol. 99, no. 12, pp. 7821–7826, 2002.
- [16] P. W. Holland, K. B. Laskey, and S. Leinhardt, “Stochastic block-models: First steps,” *Social networks*, vol. 5, no. 2, pp. 109–137, 1983.
- [17] B. Perozzi, R. Al-Rfou, and S. Skiena, “Deepwalk: Online learning of social representations,” in *Proceedings of the 20th ACM SIGKDD international conference on Knowledge discovery and data mining*, pp. 701–710, 2014.
- [18] A. Grover and J. Leskovec, “node2vec: Scalable feature learning for networks,” in *Proceedings of the 22nd ACM SIGKDD international conference on Knowledge discovery and data mining*, pp. 855–864, 2016.
- [19] W. L. Hamilton, R. Ying, and J. Leskovec, “Representation learning on graphs: Methods and applications,” *IEEE Data Eng. Bull.*, vol. 40, no. 3, pp. 52–74, 2017.

- [20] M. Ou, P. Cui, J. Pei, Z. Zhang, and W. Zhu, "Asymmetric transitivity preserving graph embedding," in *Proceedings of the 22nd ACM SIGKDD international conference on Knowledge discovery and data mining*, pp. 1105–1114, 2016.
- [21] S. Cao, W. Lu, and Q. Xu, "Grarep: Learning graph representations with global structural information," in *Proceedings of the 24th ACM international conference on information and knowledge management*, pp. 891–900, 2015.
- [22] T. N. Kipf and M. Welling, "Variational graph auto-encoders," *arXiv preprint arXiv:1611.07308*, 2016.
- [23] S. Zhang, H. Tong, J. Xu, and R. Maciejewski, "Graph convolutional networks: a comprehensive review," *Computational Social Networks*, vol. 6, no. 1, pp. 1–23, 2019.
- [24] S. Bonner, I. Kureshi, J. Brennan, G. Theodoropoulos, A. S. McGough, and B. Obara, "Exploring the Semantic Content of Unsupervised Graph Embeddings: An Empirical Study," *Data Science and Engineering*, vol. 4, pp. 269–289, Sept. 2019.
- [25] S. Khoshraftar, S. Mahdavi, and A. An, "Centrality-based Interpretability Measures for Graph Embeddings," in *2021 IEEE 8th International Conference on Data Science and Advanced Analytics (DSAA)*, pp. 1–10, Oct. 2021.
- [26] Y. Wang, Y. Yao, H. Tong, F. Xu, and J. Lu, "Discerning edge influence for network embedding," in *Proceedings of the 28th ACM International Conference on Information and Knowledge Management*, pp. 429–438, 2019.
- [27] H. Park, "Providing post-hoc explanation for node representation learning models through inductive conformal predictions," *IEEE Access*, 2022.
- [28] C. T. Duong, T. T. Nguyen, T.-D. Hoang, H. Yin, M. Weidlich, and Q. V. H. Nguyen, "Deep mincut: Learning node embeddings by detecting communities," *Pattern Recognition*, vol. 134, p. 109126, 2023.
- [29] B. Rozemberczki, R. Davies, R. Sarkar, and C. Sutton, "GEMSEC: graph embedding with self clustering," in *Proceedings of the 2019 IEEE/ACM International Conference on Advances in Social Networks Analysis and Mining*, (Vancouver British Columbia Canada), pp. 65–72, ACM, Aug. 2019.
- [30] X. Wang, P. Cui, J. Wang, J. Pei, W. Zhu, and S. Yang, "Community Preserving Network Embedding," *Proceedings of the AAAI Conference on Artificial Intelligence*, vol. 31, Feb. 2017.
- [31] B. Kang, J. Lijffijt, and T. De Bie, "Explaine: An approach for explaining network embedding-based link predictions," *arXiv preprint arXiv:1904.12694*, 2019.
- [32] S. Zhang, J. Zhang, X. Song, S. Adeshina, D. Zheng, C. Faloutsos, and Y. Sun, "Page-link: Path-based graph neural network explanation for heterogeneous link prediction," in *Proceedings of the ACM Web Conference 2023*, pp. 3784–3793, 2023.
- [33] Z. Wang, B. Zong, and H. Sun, "Modeling context pair interaction for pairwise tasks on graphs," in *Proceedings of the 14th ACM International Conference on Web Search and Data Mining*, pp. 851–859, 2021.
- [34] A. Rossi, D. Firmani, P. Merialdo, and T. Teofili, "Explaining link prediction systems based on knowledge graph embeddings," in *Proceedings of the 2022 International Conference on Management of Data*, pp. 2062–2075, 2022.
- [35] W. Zhang, B. Paudel, W. Zhang, A. Bernstein, and H. Chen, "Interaction embeddings for prediction and explanation in knowledge graphs," in *Proceedings of the Twelfth ACM International Conference on Web Search and Data Mining*, pp. 96–104, 2019.
- [36] T. Prouteau, N. Dugué, N. Camelin, and S. Meignier, "Are embedding spaces interpretable? results of an intrusion detection evaluation on a large french corpus," in *LREC 2022*, 2022.
- [37] L. K. Şenel, I. Utlu, V. Yücesoy, A. Koc, and T. Cukur, "Semantic structure and interpretability of word embeddings," *IEEE/ACM Transactions on Audio, Speech, and Language Processing*, vol. 26, no. 10, pp. 1769–1779, 2018.
- [38] J. Shin, A. Madotto, and P. Fung, "Interpreting word embeddings with eigenvector analysis," in *32nd Conference on Neural Information Processing Systems (NIPS 2018)*, IRASL workshop, 2018.
- [39] S. Park, J. Bak, and A. Oh, "Rotated Word Vector Representations and their Interpretability," in *Proceedings of the 2017 Conference on Empirical Methods in Natural Language Processing*, (Copenhagen, Denmark), pp. 401–411, Association for Computational Linguistics, Sept. 2017.
- [40] P. P. Liang, M. Zaheer, Y. Wang, and A. Ahmed, "Anchor & Transform: Learning Sparse Embeddings for Large Vocabularies," *arXiv:2003.08197 [cs, stat]*, Mar. 2021. arXiv: 2003.08197.
- [41] F. Sun, J. Guo, Y. Lan, J. Xu, and X. Cheng, "Sparse word embeddings using l1 regularized online learning," in *Proceedings of the twenty-fifth international joint conference on artificial intelligence*, pp. 2915–2921, 2016.
- [42] H. Luo, Z. Liu, H. Luan, and M. Sun, "Online Learning of Interpretable Word Embeddings," in *Proceedings of the 2015 Conference on Empirical Methods in Natural Language Processing*, (Lisbon, Portugal), pp. 1687–1692, Association for Computational Linguistics, Sept. 2015.
- [43] A. Subramanian, D. Pruthi, H. Jhamtani, T. Berg-Kirkpatrick, and E. Hovy, "SPINE: SParse Interpretable Neural Embeddings," *Proceedings of the AAAI Conference on Artificial Intelligence*, vol. 32, Apr. 2018. Number: 1.
- [44] Y. Chen and M. J. Zaki, "KATE: K-Competitive Autoencoder for Text," in *Proceedings of the 23rd ACM SIGKDD International Conference on Knowledge Discovery and Data Mining*, (Halifax NS Canada), pp. 85–94, ACM, Aug. 2017.
- [45] M. Faruqui, Y. Tsvetkov, D. Yogatama, C. Dyer, and N. Smith, "Sparse Overcomplete Word Vector Representations," *arXiv:1506.02004 [cs]*, June 2015. arXiv: 1506.02004.
- [46] V. Belle and I. Papantonis, "Principles and practice of explainable machine learning," *Frontiers in big Data*, p. 39, 2021.
- [47] A. Datta, S. Sen, and Y. Zick, "Algorithmic transparency via quantitative input influence: Theory and experiments with learning systems," in *2016 IEEE symposium on security and privacy (SP)*, pp. 598–617, IEEE, 2016.
- [48] J. Li, W. Monroe, and D. Jurafsky, "Understanding neural networks through representation erasure," *arXiv preprint arXiv:1612.08220*, 2016.
- [49] L. S. Shapley, "17. a value for n-person games," in *Contributions to the Theory of Games (AM-28), Volume II*, pp. 307–318, Princeton University Press, 2016.
- [50] E. Štrumbelj and I. Kononenko, "Explaining prediction models and individual predictions with feature contributions," *Knowledge and information systems*, vol. 41, no. 3, pp. 647–665, 2014.
- [51] J. Castro, D. Gómez, and J. Tejada, "Polynomial calculation of the shapley value based on sampling," *Computers & Operations Research*, vol. 36, no. 5, pp. 1726–1730, 2009.
- [52] K. Aas, M. Jullum, and A. Løland, "Explaining individual predictions when features are dependent: More accurate approximations to shapley values," *Artificial Intelligence*, vol. 298, p. 103502, 2021.
- [53] H. Yuan, H. Yu, S. Gui, and S. Ji, "Explainability in graph neural networks: A taxonomic survey," *arXiv preprint arXiv:2012.15445*, 2020.
- [54] T. Funke, M. Khosla, M. Rathee, and A. Anand, "Zorro: Valid, sparse, and stable explanations in graph neural networks," *IEEE Transactions on Knowledge and Data Engineering*, 2022.
- [55] P. Baldi, "Autoencoders, unsupervised learning, and deep architectures," in *Proceedings of ICML workshop on unsupervised and transfer learning*, pp. 37–49, JMLR Workshop and Conference Proceedings, 2012.
- [56] J. Yang and J. Leskovec, "Overlapping community detection at scale: a nonnegative matrix factorization approach," in *Proceedings of the sixth ACM international conference on Web search and data mining*, pp. 587–596, 2013.
- [57] N. Bansal, X. Chen, and Z. Wang, "Can we gain more from orthogonality regularizations in training deep networks?," *Advances in Neural Information Processing Systems*, vol. 31, 2018.
- [58] E. Massart, "Orthogonal regularizers in deep learning: how to handle rectangular matrices?," in *2022 26th International Conference on Pattern Recognition (ICPR)*, pp. 1294–1299, IEEE, 2022.
- [59] N. Schaaf, M. Huber, and J. Maucher, "Enhancing decision tree based interpretation of deep neural networks through l1-orthogonal regularization," in *2019 18th IEEE International Conference On Machine Learning And Applications (ICMLA)*, pp. 42–49, IEEE, 2019.
- [60] I. Higgins, D. Amos, D. Pfau, S. Racaniere, L. Matthey, D. Rezende, and A. Lerchner, "Towards a definition of disentangled representations," *arXiv preprint arXiv:1812.02230*, 2018.
- [61] I. Higgins, L. Matthey, A. Pal, C. Burgess, X. Glorot, M. Botvinick, S. Mohamed, and A. Lerchner, "beta-vae: Learning basic visual concepts with a constrained variational framework," in *International conference on learning representations*, 2016.
- [62] J. Cha and J. Thiyaalingam, "Orthogonality-enforced latent space in autoencoders: An approach to learning disentangled representations," in *Proceedings of the 40th International Conference on Machine Learning* (A. Krause, E. Brunskill, K. Cho, B. Engelhardt, S. Sabato,

and J. Scarlett, eds.), vol. 202 of *Proceedings of Machine Learning Research*, pp. 3913–3948, PMLR, 23–29 Jul 2023.

- [63] Y. Song, N. Sebe, and W. Wang, “Orthogonal svd covariance conditioning and latent disentanglement,” *IEEE Transactions on Pattern Analysis and Machine Intelligence*, 2022.
- [64] F. M. Bianchi, D. Grattarola, and C. Alippi, “Spectral clustering with graph neural networks for graph pooling,” in *International Conference on Machine Learning*, pp. 874–883, PMLR, 2020.
- [65] R. Yang, J. Shi, X. Xiao, Y. Yang, J. Liu, and S. S. Bhowmick, “Scaling attributed network embedding to massive graphs,” *arXiv preprint arXiv:2009.00826*, 2020.
- [66] L. Peel, D. B. Larremore, and A. Clauset, “The ground truth about metadata and community detection in networks,” *Science advances*, vol. 3, no. 5, p. e1602548, 2017.
- [67] D. Hric, R. K. Darst, and S. Fortunato, “Community detection in networks: Structural communities versus ground truth,” *Physical Review E*, vol. 90, no. 6, p. 062805, 2014.
- [68] Z. Ding, X. Zhang, D. Sun, and B. Luo, “Overlapping community detection based on network decomposition,” *Scientific reports*, vol. 6, no. 1, pp. 1–11, 2016.
- [69] S. Fortunato, “Community detection in graphs,” *Physics reports*, vol. 486, no. 3–5, pp. 75–174, 2010.
- [70] Y.-Y. Ahn, J. P. Bagrow, and S. Lehmann, “Link communities reveal multiscale complexity in networks,” *nature*, vol. 466, no. 7307, pp. 761–764, 2010.
- [71] T. S. Evans and R. Lambiotte, “Line graphs, link partitions, and overlapping communities,” *Physical Review E*, vol. 80, no. 1, p. 016105, 2009.
- [72] V. D. Blondel, J.-L. Guillaume, R. Lambiotte, and E. Lefebvre, “Fast unfolding of communities in large networks,” *Journal of statistical mechanics: theory and experiment*, vol. 2008, no. 10, p. P10008, 2008.
- [73] M. Du, N. Liu, and X. Hu, “Techniques for interpretable machine learning,” *Communications of the ACM*, vol. 63, no. 1, pp. 68–77, 2019.
- [74] B. Perozzi, V. Kulkarni, H. Chen, and S. Skiena, “Don’t walk, skip! online learning of multi-scale network embeddings,” in *Proceedings of the 2017 IEEE/ACM International Conference on Advances in Social Networks Analysis and Mining 2017*, pp. 258–265, 2017.
- [75] A. Clauset, C. Moore, and M. E. Newman, “Hierarchical structure and the prediction of missing links in networks,” *Nature*, vol. 453, no. 7191, pp. 98–101, 2008.



Simone Piaggese received his Ph.D. degree in Data Science and Computation from the University of Bologna, Italy, in 2023. He is currently a Post-Doctoral Fellow in the Computer Science department of the University of Pisa, Italy. His research interests include interpretability of graph learning models.



Megha Khosla is an Assistant Professor in the Intelligent Systems department at TU Delft, Netherlands. Her main research area is Machine Learning on Graphs with focus on three key aspects of effectiveness, interpretability and privacy-preserving learning.



André Panisson is a Principal Researcher in the CENTAI Institute in Turin, Italy. His current research focuses on the development of tools to facilitate the explainability, fairness, and transparency of Artificial Intelligence systems. His past and current research also focuses on the intersection of Machine Learning, Network Science, and Data Science, primarily on developing methods for the analysis, modeling, and simulation of complex phenomena in systems that involve technological and social factors.



Avishek Anand is an associate professor in the Web Information Systems (WIS) at the Software Technology (ST) department at Delft University of Technology (TU Delft). He is also a member of the L3S Research Center, Hannover, Germany. One of his main research focus is interpretability of machine learning models with focus on representations from discrete input like text and graphs.

APPENDIX

Extensive Results

In Figures A1, A2 and A3 we report the whole results on multiple datasets for our experiments, that were only shown for CORA in the main paper (Figures 4-6).

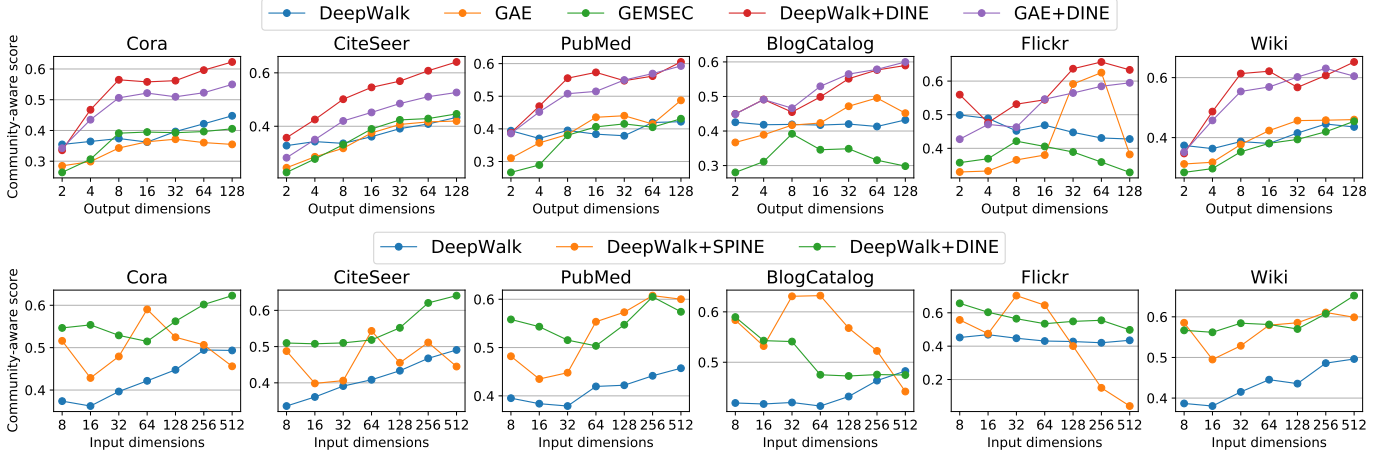


Fig. A1: Community-aware scores for the interpretations of embeddings trained with different methods. In the top panel, we compare the community-aware scores of different dense embedding methods when varying the number of output dimensions and choosing the best score among models with different number of input dimensions; in the bottom panel, we compare the scores of DEEPWALK and SPINE when varying the number of input dimensions and choosing the best score among models with a different number of output dimensions.

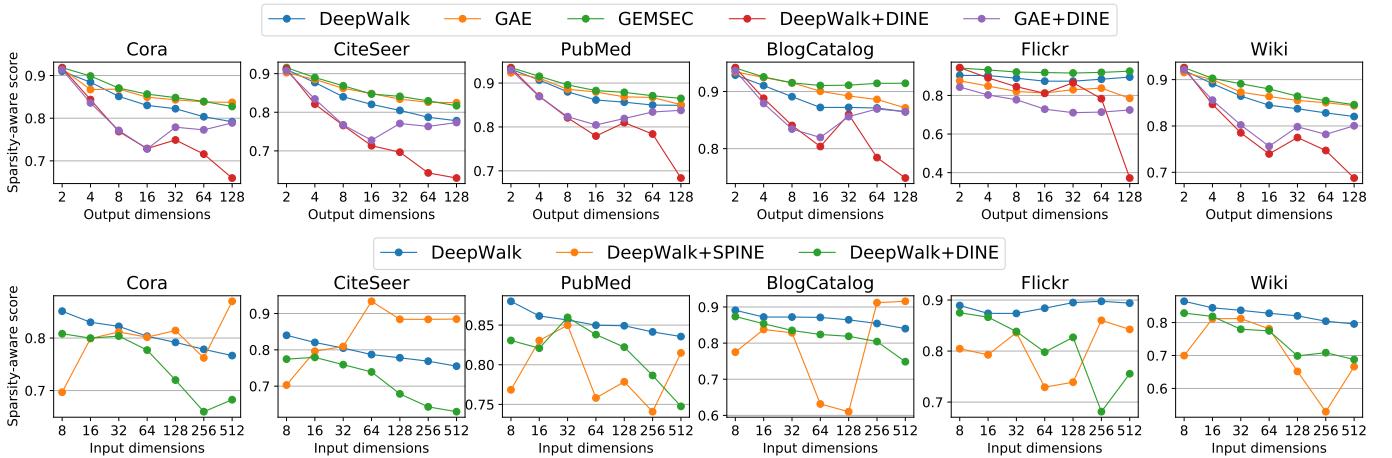


Fig. A2: Sparsity-aware scores for the interpretations of embeddings trained with different methods. In the top panel, we compare the sparsity-aware scores of different dense embedding methods when varying the number of output dimensions and choosing the best score among models with different number of input dimensions; in the bottom panel, we compare the scores of DEEPWALK and SPINE when varying the number of input dimensions and choosing the best score among models with a different number of output dimensions.

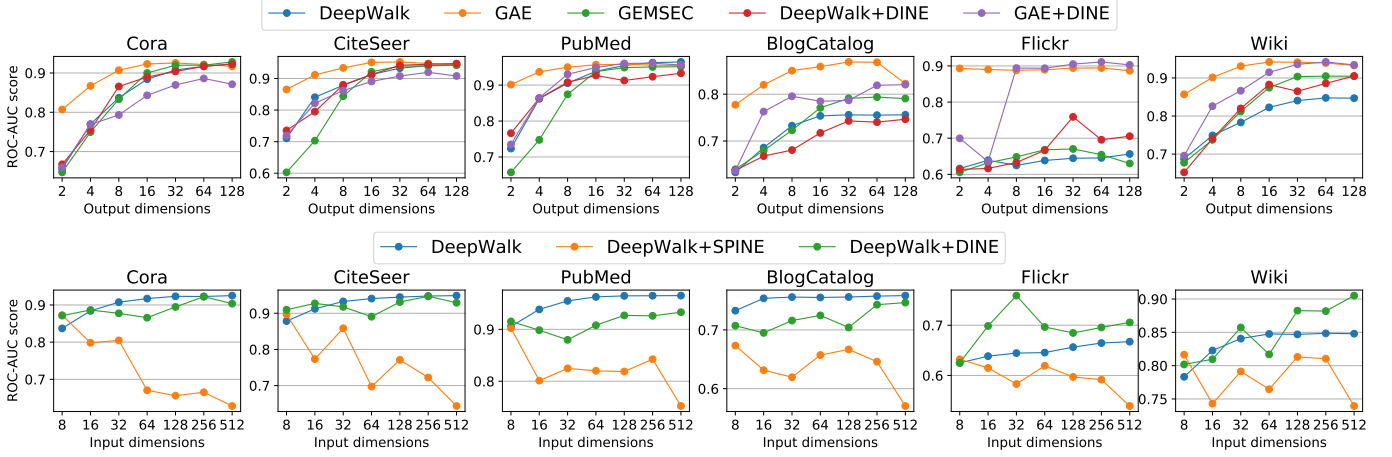


Fig. A3: ROC-AUC scores in link prediction tasks of embeddings trained with different methods. In the top panel, we compare the ROC-AUC scores of different dense embedding methods when varying the number of output dimensions and choosing the best score among models with a different number of input dimensions; in the bottom panel, we compare the scores of DEEPWALK and SPINE when varying the number of input dimensions and choosing the best score among models with a different number of output dimensions.

Ablation Studies

In Figure A4 we show the interpretability metrics on multiple datasets when removing regularizers from the DINE objective.

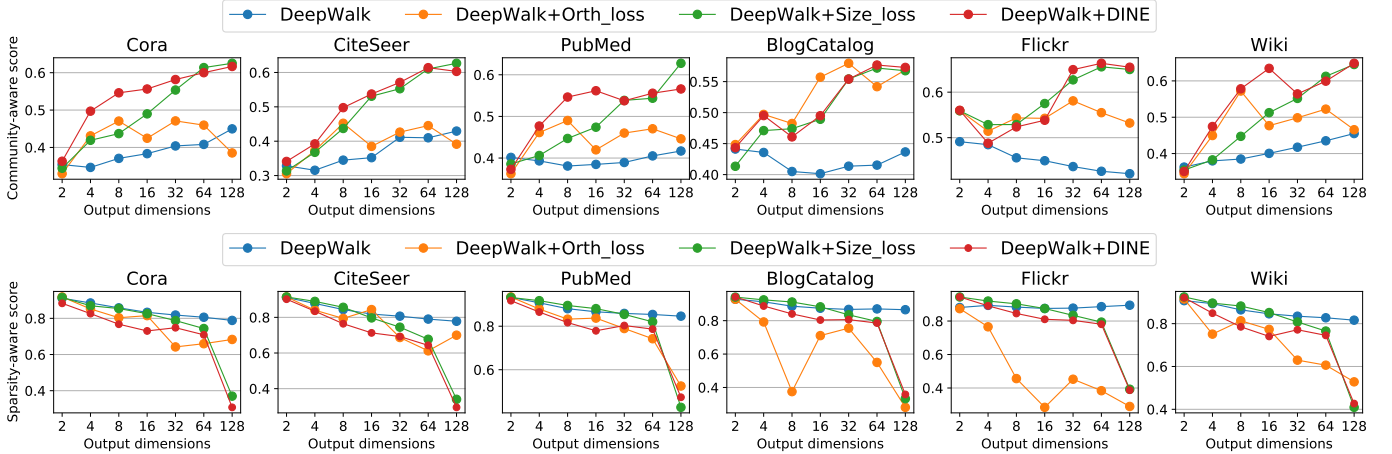


Fig. A4: Interpretability scores for the DINE embeddings trained on DEEPWALK vectors when removing regularizers (*Size Loss*, *Orthogonality Loss* or both), varying the number of output dimensions and choosing the best score among models with different number of input dimensions. In the top panel, we compare the community-aware scores; in the bottom panel, we compare sparsity-aware scores.

Noise Robustness Studies

In Figure A5 we show the interpretability metrics on multiple datasets when adding random noise to the entries of DEEPWALK embedding matrices. For each entry $X_{d,v} = v_d$ we sample a random Gaussian variable $\epsilon_{d,v} \propto \mathcal{N}(0, \delta)$, where the variance δ represents the amount of noise that we want to add. Then, we perturb the original embedding entries with the following rule $\tilde{X}_{d,v} = X_{d,v} \cdot \exp \epsilon_{d,v}$.

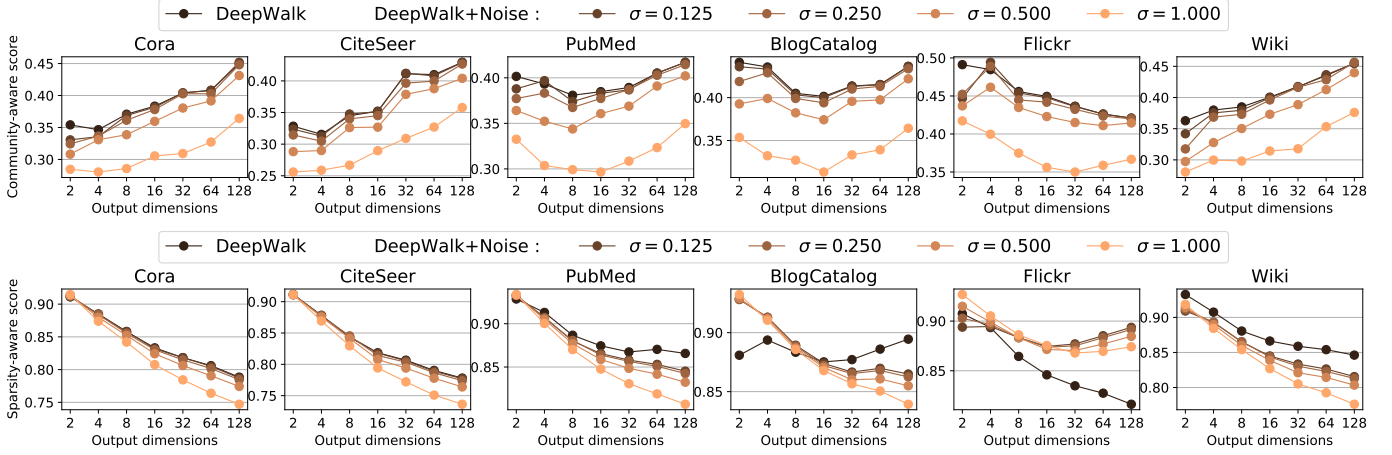


Fig. A5: Interpretability scores for the DEEPWALK embeddings perturbed with variable entry-wise noise, varying the number of output dimensions and choosing the best score among models with different number of input dimensions. In the top panel, we compare the community-aware scores; in the bottom panel, we compare sparsity-aware scores.